A growing braking index and spin-down swings for the pulsar PSR B0540−69

Cristóbal M. Espinoza,[1,2] Lucien Kuiper,[3] Wynn C. G. Ho,[4] Danai Antonopoulou,[5] Zaven Arzoumanian,[6] Alice K. Harding,[7] Paul S. Ray,[8] and George Younes[9]

[1]*Departamento de Física, Universidad de Santiago de Chile* (USACH), *Chile*
[2]*Center for Interdisciplinary Research in Astrophysics and Space Sciences* (CIRAS), USACH, *Chile*
[3]*SRON-Netherlands Institute for Space Research, The Netherlands*
[4]*Department of Physics and Astronomy, Haverford College, USA*
[5]*Jodrell Bank Centre for Astrophysics, Department of Physics and Astronomy, The University of Manchester, UK*
[6]*X-Ray Astrophysics Laboratory, NASA Goddard Space Flight Center, USA*
[7]*Theoretical Division, Los Alamos National Laboratory, USA*
[8]*Space Science Division, U.S. Naval Research Laboratory, Washington, USA*
[9]*Astrophysics Science Division, NASA Goddard Space Flight Center, USA*

ABSTRACT

The way pulsars spin down is not understood in detail, but a number of possible physical mechanisms produce a spin-down rate that scales as a power of the rotation rate ($\dot{\nu} \propto -\nu^n$), with the power-law index n called the braking index. PSR B0540−69 is a pulsar that in 2011, after 16 years of spinning down with a constant braking index of 2.1, experienced a giant spin-down change and a reduction of its braking index to nearly zero. Here, we show that following this episode the braking index monotonically increased during a period of at least four years and stabilised at ~ 1.1. We also present an alternative interpretation of a more modest rotational irregularity that occurred in 2023, which was modelled as an anomalous negative step of the rotation rate. Our analysis shows that the 2023 observations can be equally well described as a transient swing of the spin-down rate (lasting ~ 65 days), and the Bayesian evidence indicates that this model is strongly preferred.

Keywords: Compact objects(288) — Neutron stars(1108) — Pulsars(1306) — Rotation powered pulsars(1408)

1. INTRODUCTION

The rotation rates of isolated pulsars decrease gradually over timescales that range from thousands to millions of years, due to electromagnetic radiation, plasma flows, and the emission of gravitational waves. The observed rates of loss of rotational kinetic energy, or spin-down luminosity $\dot{E} = -4\pi^2 I \nu \dot{\nu}$, cover more than eight orders of magnitude and can be as high as $10^{38}\,\mathrm{erg\,s^{-1}}$ for the youngest pulsars. Above, ν is the spin frequency, $\dot{\nu}$ is its first time derivative ($\dot{\nu} < 0$), and the moment of inertia is taken to have a typical value of $I = 10^{45}\,\mathrm{g\,cm^{-2}}$ (e.g., Lorimer & Kramer 2004). It is customary to assume a power-law scaling for the spin-down $\dot{\nu}$ as

$$\dot{\nu} = -k\nu^n \quad , \qquad (1)$$

Corresponding author: Cristóbal M. Espinoza
cristobal.espinoza.r@usach.cl

in which n is called the braking index and k depends on stellar parameters. The braking index is expected to be $n \simeq 3$ if electromagnetic radiation from a rotating dipole in vacuum dominates the spin-down, acceleration of particle winds will give $n \simeq 1$, and emission of gravitational waves predicts values $n > 3$ (Harding et al. 1999; Glampedakis & Gualtieri 2018).

The braking index n can be estimated from observations as $n = \nu \ddot{\nu}/\dot{\nu}^2$, assuming k constant, and provided the very small $\ddot{\nu}$ is reliably measured. Irregularities of the generally stable pulsar spindown occur in all pulsars to some degree and contaminate measurements of the long-term $\ddot{\nu}$. Timing noise, a continuous wandering of the rotation with respect to a simple spin-down model, is a widespread phenomenon and can cause the observed $\ddot{\nu}$ to vary widely from negative to positive values (Hobbs et al. 2010). In a number of cases, timing noise was found to consist of transitions between distinct

states, characterised by different emission properties and a different spin-down rate $\dot{\nu}$ (Lyne et al. 2010). Other irregularities, more common to young pulsars, are spin-up glitches: sporadic, sudden, and very fast increases of the rotation rate ($\Delta\nu > 0$ changes) usually accompanied by an abrupt spindown rate decrease ($\Delta\dot{\nu} < 0$) (Antonopoulou et al. 2022). Glitches are followed by relaxation of the rotational parameters over timescales of weeks to years, and this recovery often induces high values of $\ddot{\nu}$ (Liu et al. 2024). The few $\ddot{\nu}$ measurements available that might reflect the underlying, long-term behaviour indicate braking indices of different values and less than three (e.g., Livingstone et al. 2007; Espinoza et al. 2017; Parthasarathy et al. 2020). A number of processes have been suggested to explain the observed $n < 3$, from strong spindown contributions by energetic stellar winds (for which $n = 1$), to magnetic field evolution or progressive decoupling of internal superfluid components (e.g., Blandford & Romani 1988; Ho & Andersson 2012; Ho 2015; Ekşi 2017; Espinoza et al. 2017; Wang et al. 2020).

PSR B0540−69 (PSR J0540−6919) is an energetic, young, X-ray pulsar in the Large Magellanic Cloud that rotates with a period of 50 ms ($\nu \sim 20$ Hz). It exhibits the third largest known spin-down luminosity, $\dot{E} = 2 \times 10^{38}\,\mathrm{erg\,s^{-1}}$, which is likely to be the energy source of a bright synchrotron nebula that surrounds the pulsar and is visible from the radio waves to X-rays (Ge et al. 2019; Xie et al. 2024). Considering only electromagnetic dipole radiation (for which $n = 3$), the orthogonal component of the dipolar magnetic field at the surface is found as $B = 3.2 \times 10^{19}\sqrt{-\dot{\nu}/\nu^3}$. For PSR B0540−69 this leads to $B \sim 6 \times 10^{12}$ G, which is, to some degree, high but still in the range of inferred dipole fields of rotationally-powered pulsars ($10^{11} - 10^{13}$ G). This pulsar is often compared to the Crab pulsar, another young and energetic object with a standard dipole field strength and similar rotational parameters, which also powers a luminous pulsar wind nebula (PWN). However, the rotational behaviours of the Crab pulsar and PSR B0540−69 are nothing alike.

For about 16 yr, from February 1996 to late 2011, PSR B0540−69 had a stable rotational evolution with a braking index of 2.13 ± 0.01 (Zhang et al. 2001; Livingstone et al. 2007; Ferdman et al. 2015). This regular spindown was only interrupted twice, by small glitches and their associated negative $\dot{\nu}$ steps (of $\sim 0.01\%$ of $\dot{\nu}$) which had no visible recovery. Such behaviour is not unusual for pulsars with similar properties, and indeed, the Crab pulsar has mostly small to intermediate size glitches and otherwise evolves with a rather stable braking index close to 2.5 (Lyne et al. 2015). Then in December 2011, extraordinarily, PSR B0540−69 began spinning down much faster than before, with $\dot{\nu}$ decreasing by about 36% (Marshall et al. 2015). This enormous change was unexpected and did not appear related to a glitch: the spin frequency showed no change, and the measured $\Delta\dot{\nu}/\dot{\nu}$ was 10 to 100 times larger than the typical known $\dot{\nu}$ changes due to glitches. Instead, the observed spin-down rate change could have been driven by magnetospheric changes, as there are reports of brightening of the PWN at the time of the spin-down event (Ge et al. 2019). Unfortunately, there were no pulse profile or pulsed emission changes detected during this event (or any other time) which could confirm involvement of the magnetosphere (Ferdman et al. 2015; Marshall et al. 2015; Ge et al. 2019; Tuo et al. 2024). Following the 2011 $\dot{\nu}$-drop, the braking index was considerably reduced: it was measured to be $n = 0.03 \pm 0.01$ using a 480-days post-event dataset (Marshall et al. 2016), and $n = 0.163 \pm 0.001$ using a 1100-days data span (Kim & An 2019). An increasing trend, from $n = 0.1 \pm 0.1$ to $n = 1.2 \pm 0.2$ was reported by Wang et al. (2020) analysing shorter shorter intervals over an extended 1500 days postevent data set.

More recently, Tuo et al. (2024) reported another rotational episode, which occurred in July 2023. The event was described as small decreases in both the frequency and the spin-down rate, i.e., an *antiglitch* in spin frequency, but accompanied with a glitch-like change of the spin-down rate. In this letter, we present the rotational evolution of PSR B0540−69 over the last 9.4 years, from February 2015 until July 2024, describe its braking index behaviour, and re-analyse the 2023 event presenting a different interpretation.

2. INSTRUMENTS AND OBSERVATIONS

PSR B0540−69 was discovered in X-ray observations by Seward et al. (1984) and has subsequently been detected in the optical, UV, gamma rays, and polarised X-rays (Middleditch & Pennypacker 1985; Mignani et al. 2019; Fermi LAT Collaboration et al. 2015; Xie et al. 2024). Its radio emission is very faint: 0.1 mJy in the MeerKAT L-band (856-1712 MHz) (Manchester et al. 1993; Johnston & Romani 2003; Geyer et al. 2021), hence all timing observations of this pulsar are performed in the X-rays, most notably by the Rossi X-ray Timing Explorer (RXTE, Ferdman et al. 2015). After the decommissioning of RXTE on January 2012, Swift-XRT (Burrows et al. 2005) took on monitoring of PSR B0540−69 for about four years starting on February 2015 and ending on February 2019. This campaign started 3.1 years after the last RXTE observation, on Dec. 31, 2011; and is comprised of 78 observa-

tions performed at monthly cadence with typical exposure times of 0.5-2.5 ks, resulting in a total accumulated (screened) exposure time of 134.2 ks. The XRT operated in WT-mode providing a time resolution of 1.7675 ms, amply sufficient to study the timing behaviour of PSR B0540−69.

NICER (the Neutron Star Interior Composition Explorer Mission, Gendreau et al. 2016) started monitoring observations of PSR B0540−69 soon after its launch, on July 25, 2017, and it currently still executes observations of typically 0.5-2 ks at a weekly cadence. The total accumulated screened exposure time up to and including July 29, 2024 is about 110.4 ks. The NICER monitoring observations show three large data gaps: I) Mar. 24, 2018 – Mar. 20, 2019 , II) Jan. 22, 2021 – Oct. 24, 2021 and III) Mar. 18, 2022 – Jan. 19, 2023. Fortunately the first gap had full coverage by concurrent Swift-XRT observations, so it is still possible to explore the timing characteristics during that period. At the end of the third NICER data gap on Dec. 29, 2022 long polarimetric X-ray (1-8 keV) observations by IXPE (Weisskopf et al. 2022) had been initiated. The last of the three observation clusters ended on May 12, 2023, overlapping with the NICER monitoring program. In total, 2.686 Ms of screened exposure time had been accumulated with IXPE.

3. TIMING ANALYSIS AND RESULTS

We used the aforementioned X-ray observations, from February 2015 to May 2024, to measure pulse arrival times (ToAs) according to the method outlined in Sect. 4.1 of Kuiper & Hermsen (2009). These ToAs were subsequently used for the timing analysis of the next two subsections. Local fits to model the pulsar rotation close to a reference time t_0 are based on a Taylor expansion of the rotational phase, as

$$\phi(t) = \nu_0(t-t_0) + \frac{1}{2}\dot{\nu}_0(t-t_0)^2 + \frac{1}{6}\ddot{\nu}_0(t-t_0)^3 + \cdots \quad (2)$$

and were performed using the pulsar software TEMPO2 (Hobbs et al. 2006).

3.1. *The braking index evolution*

Figure 1 illustrates the evolution of the spin-down rate $\dot{\nu}$, the second frequency derivative $\ddot{\nu}$, and the inferred braking index n over the last 9.4 years. The datapoints are calculated from fits of Eq. 2 over shorter time spans and, whilst their exact values are sensitive to the choice of parameters such as interval length and number of ToAs per fit (see figure caption for details), the results are qualitatively robust.

Initially, the spin-down rate evolves under a rapidly growing $\ddot{\nu}$ for about four years. During this phase, the
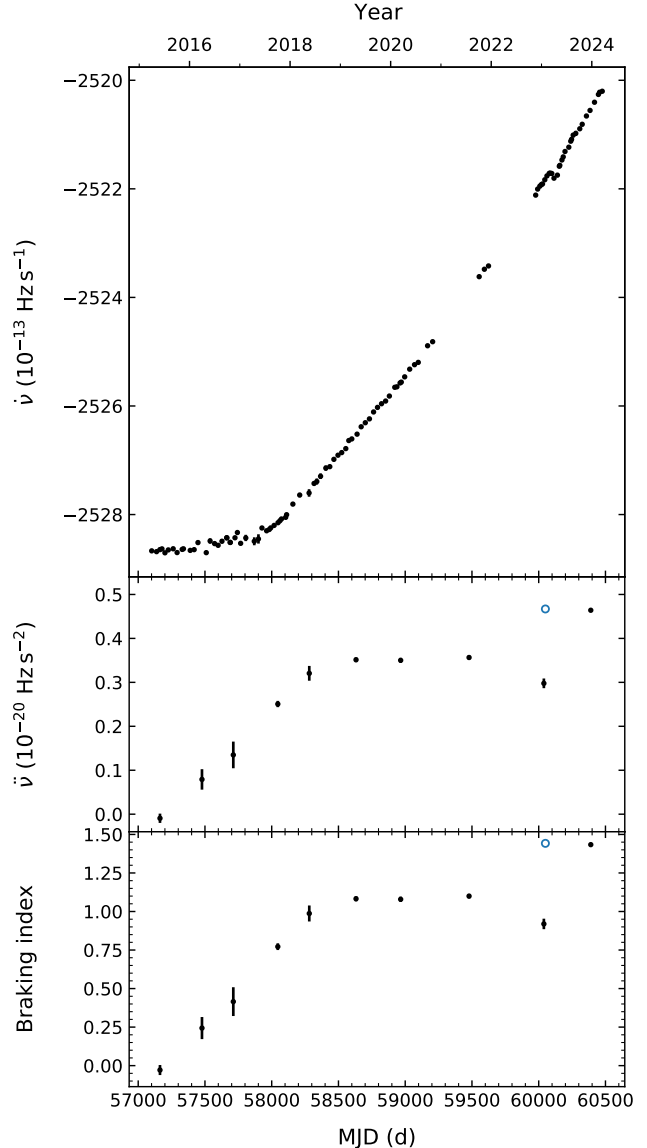

Figure 1. The evolution of $\dot{\nu}$ of PSR B0540−69 between February 2015 and May 2024. *Top panel*: The spin-down rate $\dot{\nu}$ measured from overlapping intervals approximately 80 d long, containing at least 6 ToAs each. The data window was moved by 10 d at each stride and for these short fits $\ddot{\nu}$ was held constant, at a value measured from a larger ToA set (spanning at least 600 d). *Middle panel*: $\ddot{\nu}$ measured over 250 d long, non-overlapping, time intervals. For these fits, a third derivative of the frequency was included in Eq. 2, which was held as a fixed parameter at a value calculated from much longer intervals. These values are very small ($\dddot{\nu} < 10^{-28}\,\mathrm{Hz\,s^{-3}}$) and model a slow increase of $\ddot{\nu}$ that is observed across the studied dataset. *Bottom panel*: The braking index $n = \nu\ddot{\nu}/\dot{\nu}^2$ calculated from each fit of the same intervals as in the middle panel. The blue, open circles in the bottom panels show measurements corrected by the 2023 timing event, according to the *TN* model in Table 1.

braking index $n = \nu\ddot{\nu}/\dot{\nu}^2$ tracks the changing $\ddot{\nu}$ and increases from zero to $n \simeq 1.1$ (middle and lower panels in Fig. 1; see also Wang et al. (2020)). Unfortunately we cannot assess whether the rotation maintained an $n \sim 0$ evolution between 2011 to 2015, or other developments had taken place. For example, a conjectural backwards extrapolation of the early trend seen in Fig. 1 would suggest a negative $\ddot{\nu}$ (and hence n) shortly before the onset of the observations presented here.

The period of increasing $\ddot{\nu}$ gave way to an approximately three years long period (2019, 2020, 2021), during which both $\ddot{\nu}$ and the braking index remain nearly constant. The change of $\ddot{\nu}$ during this stable phase is still positive, but very slow ($\dddot{\nu} \simeq (6\pm2)\times10^{-30}\,\mathrm{Hz\,s^{-3}}$). There are not enough observations available for 2022 to assess the stability of rotation during the second data gap (Fig. 1), however, the first hundred days of the resumed observations by NICER at the start of 2023 suggest that the pulsar was evolving with a slightly larger braking index, of 1.4 (not shown in Fig. 1, which only displays results for 250-d long intervals).

After that, in mid-2023, the pulsar underwent a rotational irregularity that cannot be described with a simple spin-down model as in Eq. 2 and is the focus of the next subsection. After this latest event and towards the end of our dataset, the new rotational state exhibits $n = 1.43\pm0.03$, but more data are necessary to establish the stability of this trend.

3.2. *The 2023 timing irregularity*

The irregular behaviour shortly after MJD 60000 – clearly visible in Fig. 1 – was observed by NICER and first reported by Tuo et al. (2024). The data and derived rotational parameters around this event are presented in Figure 2. The top panel displays timing residuals (defined as the difference between the observed ToAs and the model prediction) with respect to the best-fit model of Eq. 2 in the time interval between MJD 59936.3 and MJD 60105.0. The deviation from that timing model becomes apparent beyond that date, with the spin-frequency decreasing faster than predicted.

Including more terms (even up to ten time derivatives of the frequency) in Eq. 2 still fails to describe the evolution after MJD 60105 and does not produce flat residuals dispersed around zero. Panels (b) and (d) of Fig. 2 are illustrations of the frequency residuals and spin-down rate residuals with respect to the pre-event timing model, whilst panel (c) is the $\dot{\nu}$ curve. The data points for these three panels have been calculated as in Fig. 1, from overlapping segments of TOAs, therefore fast changes on timescales shorter than 80 d have been smoothed out. Nonetheless, the plots aid to visualise the
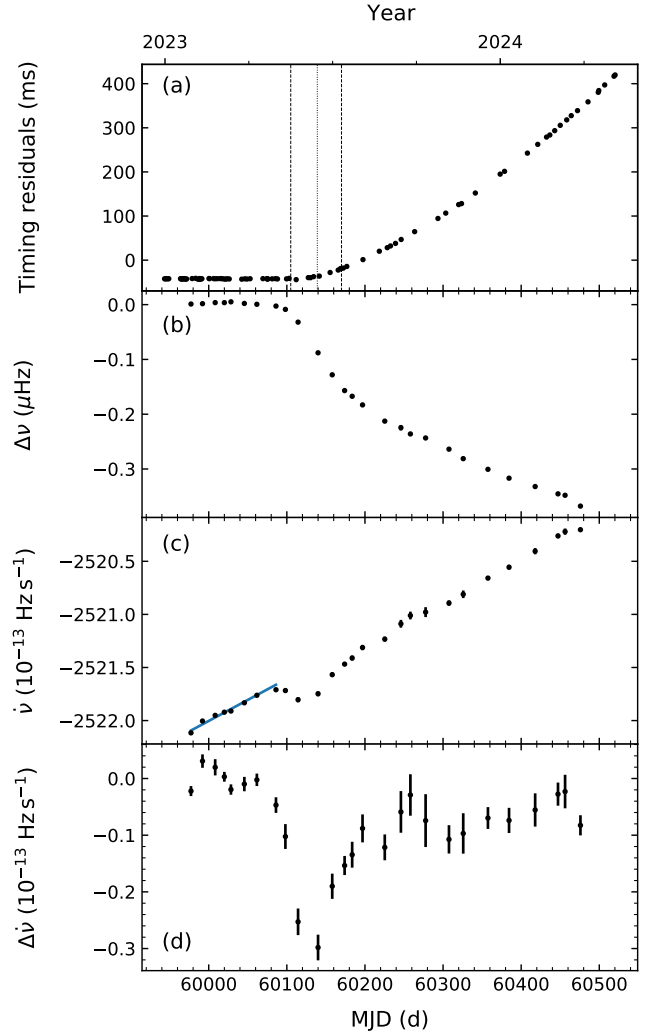

Figure 2. The rotational evolution of PSR B0540−69 since January 2023. *(a)* The timing residuals relative to a model like Eq. 2 adjusted up to MJD 60105. The two vertical segmented lines mark the epochs of the $\dot{\nu}$ changes according to the TN model (t_{g1} and t_{g2}), while the vertical dotted line indicates t_g according to the Glitch model. *(b)* Frequency residuals relative to the same model. *(c)* The behaviour of $\dot{\nu}$. The blue line represents the model used in the other panels. *(d)* The residuals of $\dot{\nu}$ relative to the same model. Frequency and spin-down rate values were calculated as in Fig. 1, thus short term features (< 80 d) have been smoothed.

main features of the rotation before, during, and after the 2023 event.

Tuo et al. (2024) modelled the irregularity as if it were a glitch, with two discontinuities in ν and $\dot{\nu}$ at MJD 60132. Their result gives a negative frequency step $\Delta\nu < 0$, and the event was named an anti-glitch because typical glitches have $\Delta\nu > 0$ (Antonopoulou et al. 2022). The spin-down rate change was found, however, to be negative ($\Delta\dot{\nu} < 0$, as usual in ordinary glitches), which implies a progressive departure of the spin ν from its ex-

pected values. In the following, we re-evaluate the glitch model and present an alternative interpretation of the event, which is more strongly supported by the data.

A basic glitch model (that is, without including a post-glitch recovery) involves instantaneous, unresolved steps in spin frequency $\Delta\nu$ and spin-down rate $\Delta\dot{\nu}$, whose effects are added to the phase defined in Eq. 2 after the glitch epoch, t_g:

$$\phi_g(t) = \Delta\phi + \Delta\nu(t - t_g) + \frac{1}{2}\Delta\dot{\nu}(t - t_g)^2 \quad , \quad (3)$$

in which $\Delta\phi$ ensures phase continuity across the event. Using our updated, longer dataset, we tested a glitch model as in Eq. 3 but were unable to obtain flat timing residuals: obvious additional signal remains if only steps in ν and $\dot{\nu}$ are considered. To obtain an adequate fit, we must include an extra term describing a non-zero $\ddot{\nu}$ change in the model of Eq. 3. The timing residuals of this model are shown as blue squares in Figure 3 and the best solution returns a frequency change of $\Delta\nu = -0.109 \pm 0.004\,\mu$Hz, in good agreement with Tuo et al. (2024).

Further inspection of the data, however, reveals that this may not be the optimal description of the event. A glitch leaves a cusp-like signature in the timing residuals –indicative of a discontinuity in spin frequency (Espinoza et al. 2011; Antonopoulou et al. 2022), contrary to the timing residuals of PSR B0540−69 in this case, which show no indication of such feature (top panel in Fig. 2). Instead, the frequency appears to change over a relatively short – yet resolved – timescale. This, combined with the fact that the spin-down rate $\dot{\nu}$ exhibits a relative decrease after MJD ~ 60100 which almost completely reverts about 100 days later (panels (c) and (d) in Fig. 2), suggest that this event could be instead driven by a spin-down swing.

To test the above hypothesis, we develop and fit a second model, in which $\dot{\nu}$ changes discretely at two different times. We call this the *TN* model, as it resembles the timing noise of some pulsars in which abrupt $\dot{\nu}$ changes produce similar features (Shaw et al. 2018). The *TN* model does not involve any sudden frequency changes, hence $\Delta\nu = 0$, and can be written as:

$$\phi_{TN}(t) = \Delta\phi_1 + \frac{1}{2}\Delta\dot{\nu}_1(t - t_{g1})^2 +$$
$$H(t - t_{g2})\left(\Delta\phi_2 + \frac{1}{2}\Delta\dot{\nu}_2(t - t_{g2})^2\right) \quad , \quad (4)$$

valid only for $t > t_{g1}$ and where H is the Heaviside function so that the second spin-down step $\Delta\dot{\nu}_2$ is added only after t_{g2}. Discrete changes of the phase ($\Delta\phi_1$ and $\Delta\phi_2$, as for the glitch model,) associated with each event
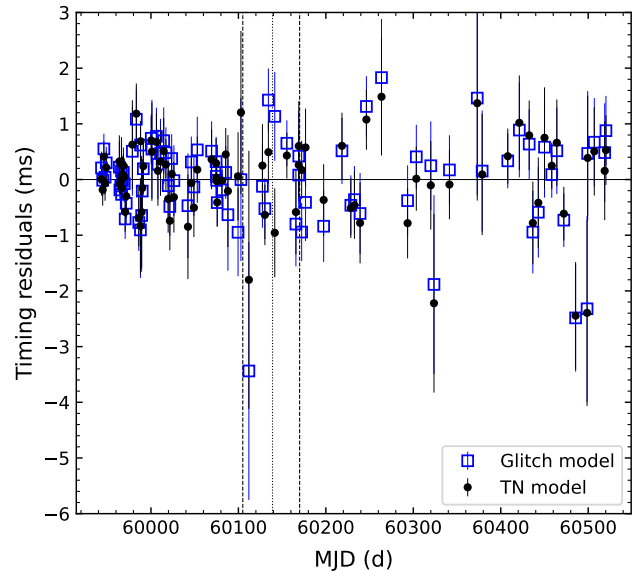

Figure 3. Timing residuals for the two models in Table 1. The vertical dotted line shows the epoch t_g for the Glitch model, while the two vertical dashed lines mark the epochs t_{g1} and t_{g2} for the TN model.

were also included, to ensure phase connection across each epoch. The residuals of this model are denoted with black circles in Fig. 3.

The following process was used to fit both the glitch and the *TN* model to the data. First, we used TEMPO2 to find the epochs (t_g for the glitch model; t_{g1} and t_{g2} for the *TN* model) that produced the smallest weighted Root Mean Square (RMS) of the timing residuals. These epochs are quoted in Table 1. In both cases the epoch(s) uncertainties are about 2-3 d, mostly reflecting the TOAs' typical separation in time. Whilst both models provide acceptable residuals, the RMS for the *TN* model ($445\,\mu$s) is somewhat smaller than the one for the glitch model ($506\,\mu$s). This can also be detected by eye in Fig. 3, however such a difference is not large enough to firmly favour one model over the other. We note though that an f-test gives a probability of 9×10^{-6}, which could be an indication that the extra parameter of the *TN* model is justified. The χ^2 and degrees of freedom (d.o.f.) for each fit are quoted in Table 1.

To draw conclusions on the preferred model, we then used a Bayesian approach to data fitting and compared the models' evidence. For this, we used the timing software package PINT (Luo et al. 2021) together with the `nestle` library[1], which uses Bayesian evidence and a

---

[1] https://github.com/kbarbary/nestle

Table 1. Inferred timing parameters of the 2023 rotational irregularity for the two models considered. Errors correspond to 68% confidence intervals of the posterior distributions.

Parameter	Glitch model	TN model
Epoch (MJD)	60050.0	60050.0
ν (Hz)	19.635893779(1)	19.635893780(1)
$\dot{\nu}$ ($10^{-10}\,\mathrm{Hz\,s^{-1}}$)	-2.521821(2)	-2.521803(2)
$\ddot{\nu}$ ($10^{-21}\,\mathrm{Hz\,s^{-2}}$)	4.2(1)	4.67(2)
Event 1 (MJD)	60139	60105
$\Delta\phi_1$	0.01(1)	0.00(1)
$\Delta\nu_1$ (μHz)	-0.109(4)	–
$\Delta\dot{\nu}_1$ ($10^{-15}\,\mathrm{Hz\,s^{-1}}$)	-5(1)	-31.2(4)
$\Delta\ddot{\nu}_1$ ($10^{-22}\,\mathrm{Hz\,s^{-2}}$)	6(1)	–
Event 2 (MJD)	–	60170
$\Delta\phi_2$	–	0.02(1)
$\Delta\dot{\nu}_2$ ($10^{-15}\,\mathrm{Hz\,s^{-1}}$)	–	21(1)
RMS (μs)	505.85	445.45
χ^2/d.o.f.	94.8/79	73.5/78
$\log(Z)$	591.24	603.71
$Z_{\mathrm{Glitch}}/Z_{TN}$	3.8×10^{-6}	
MJD range	59943.45 - 60520.27	
Number of ToAs	88	

NOTE—Event 1 epoch refers to t_g in the glitch model and to t_{g1} in the TN model. Event 2 refers to t_{g2} in the TN model. The uncertainties for these values are 2-3 d (see the text for more details).

nested sampling algorithm to explore the posterior distributions based on Feroz et al. (2009). We used 5,000 points and an evidence precision of 10^{-5}. The event epochs were held constant at the best values found before. The most likely parameter values and their 68% confidence intervals are reported in Table 1. When comparing the final evidence (Z) of the glitch model over the TN model, a Bayes factor of 3.8×10^{-6} is obtained. This result implies a strong preference for the TN model compared to the Glitch model.

4. DISCUSSION

While the TN model may at first seem unusual, it has the potential of characterising timing irregularities in terms of physical processes that are often unexplored and different from glitches. Glitches have characteristic signatures and well established shared properties that are best explained by angular momentum transfer from an interior neutron superfluid to the rest of the star, causing it to spin-up (Anderson & Itoh 1975). On the

other hand, the few reported antiglitches are typically in pulsars of high magnetic field and magnetars, each with its unique signature (Antonopoulou et al. 2022). These events are often associated with emission variations, indicating a possible magnetospheric origin or, at least, involvement. Smaller amplitude glitch-like and antiglitch-like anomalies, with $|\Delta\nu| < 0.1\,\mu$Hz, are seen in the Crab and Vela pulsar (which have inferred magnetic fields of the order 10^{12} G) and constitute a different population from their glitches (Espinoza et al. 2014, 2021).

The TN model invokes rather fast changes in the torque without the need for an instantaneous frequency decrease. Such abrupt, transient, changes of $\dot{\nu}$, or even routine switches between different values, have been seen in several pulsars (e.g., PSR B1822−09; Hobbs et al. 2010; Shaw et al. 2018). They are mostly studied when they correlate with detectable changes in the radio pulse profile (Lyne et al. 2010), and can potentially explain part of the timing noise seen in all pulsars. Indeed, Espinoza et al. (2021) showed that several irregularities in the rotation of the Vela pulsar can be described with minute, sudden, changes just in $\dot{\nu}$ (with $\Delta\nu = 0$). Moreover, PSR B0540−69 has already displayed a significant spin-down change in the past, hence it is not improbable that these smaller spin-down changes were caused by a similar physical process as the 2011 event.

We have also analysed one year of RXTE observations from 2003, and found a similar episode to the 2023 one, in which $\dot{\nu}$ at some point becomes smaller than the projection determined by $\ddot{\nu}$. The 2003 event is close to the second of the small glitches reported by Ferdman et al. (2015), for which the measured changes $\Delta\dot{\nu}$ are similar in magnitude to those we find for the 2023 timing irregularity. Our preliminary analysis indicates that the 2003 event can also be well modelled by a TN model. Is it possible that the two small glitches were instead $\dot{\nu}$ changes, rather than real glitches? We will address this question in future work, which will also aim to uncover the overall rotational history of PSR B0540−69 using archival data.

The relative magnitude of the 2011 $\dot{\nu}$ change is closer to those seen in intermittent pulsars (Kramer et al. 2006; Young et al. 2013; Marshall et al. 2015), except that so far $\dot{\nu}$ has not returned to its previous value, and might never do so if PSR B0540−69 reached a new steady state. In a sense, the collection of peculiar $\dot{\nu}$ behaviours from PSR B0540−69 resembles more the erratic behaviour of magnetars. In fact, the pulsar's current trajectory in the P-$\dot{P}$ diagram is towards the magnetars region, as determined by the current $n < 2$. Note that this trend commenced dramatically with the large

2011 $\dot{\nu}$ change, when the inferred B increased by about 10^{12} G (and the characteristic age $(-\nu/2\dot{\nu})$ decreased by 440 yr). Unfortunately, it is not possible to use radio band observations of PSR B0540−69 to better understand its torque variability and its radio emission stability.

Processes typically put forward to explain low braking indices like those observed for PSR B0540−69 in its early stable period (until 2011) include significant contributions to spin-down by outflows, or a time-varying k in Eq. 1. Such changes can arise, for example, due to magnetic field evolution in the neutron star crust or a decreasing effective moment of inertia as – early in the star's life – the interior neutrons turn superfluid. Sharp transitions though, as the large $\dot{\nu}$ drop in 2011, are most likely caused by magnetospheric variations, such as in the plasma outflow, or the overall structure e.g., the size of the open field line region. Marshall et al. (2015) explore some of these mechanisms for the PSR B0540−69 case. It is unfortunate that there is a time period of more than 1000 days without data after the 2011 giant $\dot{\nu}$ drop, which leaves unclear if and how the steady increase of $\ddot{\nu}$ and the evolving braking index shown in Fig. 1 are somehow connected to it.

Finally, note that the behaviour described for the braking index is determined by $\ddot{\nu}$ values measured over time spans which are considerably shorter than the timescale of the pulsar rotational evolution. The underlying longer-term trend is therefore still unclear. If anything, the enormous 2011 decrease in $\dot{\nu}$ has made the (discontinuous) long-term $\ddot{\nu}$ very small, if not negative.

5. FINAL REMARKS

We have demonstrated that the 2023 rotational episode seen in PSR B0540−69 can be successfully modelled either as negative steps in both frequency and spin-down rate, plus an increase in $\ddot{\nu}$, or as a transient change of the spin-down rate. The latter model, however, presents higher Bayesian evidence. Thus it may be common for PSR B0540−69 to experience variations of its spin-down rate, in the form of rapid changes in $\dot{\nu}$, or in the form of a highly varying $\ddot{\nu}$, or both. The presence of such rotational irregularities in PSR B0540−69 presents a great study opportunity because of its strong $\ddot{\nu}$ that can be accurately determined in relatively short timescales. Based on knowledge derived from radio pulsar observations, it is likely that the torque variations reflect magnetic reconfigurations or significant changes in the magnetospheric plasma density and outflow. Interestingly, PSR B0540−69 also shows an unexplained steady evolution of $\ddot{\nu}$ over a timescale of at least ~ 4 years, which resulted in its braking index changing from nearly zero to a bit over 1, though during and after the 2023 episode the new n approaches 1.5. All these rotational features are not common in typical pulsars, thus it is of utmost importance to regularly monitor PSR B0540−69 by X-ray observatories, not only to accurately follow its rotation but also its emission in order to understand the role of the magnetosphere in the observed evolution and track any variations. To that end, continued observing in the radio (even if infrequent) is also imperative, especially shortly after the detection of any more rotational irregularities.

Facilities: Swift(XRT), NICER, IXPE

Software: TEMPO2 (Hobbs et al. 2006), PINT (Luo et al. 2021), nestle (https://github.com/kbarbary/nestle)

REFERENCES

Anderson, P. W., & Itoh, N. 1975, Nature, 256, 25, doi: 10.1038/256025a0

Antonopoulou, D., Haskell, B., & Espinoza, C. M. 2022, Reports on Progress in Physics, 85, 126901, doi: 10.1088/1361-6633/ac9ced

Blandford, R. D., & Romani, R. W. 1988, MNRAS, 234, 57P, doi: 10.1093/mnras/234.1.57P

Burrows, D. N., Hill, J. E., Nousek, J. A., et al. 2005, SSRv, 120, 165, doi: 10.1007/s11214-005-5097-2

Ekşi, K. Y. 2017, MNRAS, 469, 1974, doi: 10.1093/mnras/stx1035

Espinoza, C. M., Antonopoulou, D., Dodson, R., Stepanova, M., & Scherer, A. 2021, A&A, 647, A25, doi: 10.1051/0004-6361/202039044

Espinoza, C. M., Antonopoulou, D., Stappers, B. W., Watts, A., & Lyne, A. G. 2014, MNRAS, 440, 2755, doi: 10.1093/mnras/stu395

Espinoza, C. M., Lyne, A. G., & Stappers, B. W. 2017, MNRAS, 466, 147, doi: 10.1093/mnras/stw3081

Espinoza, C. M., Lyne, A. G., Stappers, B. W., & Kramer, M. 2011, MNRAS, 414, 1679, doi: 10.1111/j.1365-2966.2011.18503.x

Ferdman, R. D., Archibald, R. F., & Kaspi, V. M. 2015, ApJ, 812, 95, doi: 10.1088/0004-637X/812/2/95

Fermi LAT Collaboration, Ackermann, M., Albert, A., et al. 2015, Science, 350, 801, doi: 10.1126/science.aac7400

Feroz, F., Hobson, M. P., & Bridges, M. 2009, MNRAS, 398, 1601, doi: 10.1111/j.1365-2966.2009.14548.x

Ge, M. Y., Lu, F. J., Yan, L. L., et al. 2019, Nature Astronomy, 3, 1122, doi: 10.1038/s41550-019-0853-5

Gendreau, K. C., Arzoumanian, Z., Adkins, P. W., et al. 2016, in Society of Photo-Optical Instrumentation Engineers (SPIE) Conference Series, Vol. 9905, Space Telescopes and Instrumentation 2016: Ultraviolet to Gamma Ray, ed. J.-W. A. den Herder, T. Takahashi, & M. Bautz, 99051H, doi: 10.1117/12.2231304

Geyer, M., Serylak, M., Abbate, F., et al. 2021, MNRAS, 505, 4468, doi: 10.1093/mnras/stab1501

Glampedakis, K., & Gualtieri, L. 2018, in Astrophysics and Space Science Library, Vol. 457, Astrophysics and Space Science Library, ed. L. Rezzolla, P. Pizzochero, D. I. Jones, N. Rea, & I. Vidaña, 673, doi: 10.1007/978-3-319-97616-7_12

Harding, A. K., Contopoulos, I., & Kazanas, D. 1999, ApJL, 525, L125, doi: 10.1086/312339

Ho, W. C. G. 2015, MNRAS, 452, 845, doi: 10.1093/mnras/stv1339

Ho, W. C. G., & Andersson, N. 2012, Nature Physics, 8, 787, doi: 10.1038/nphys2424

Hobbs, G., Lyne, A. G., & Kramer, M. 2010, MNRAS, 402, 1027, doi: 10.1111/j.1365-2966.2009.15938.x

Hobbs, G. B., Edwards, R. T., & Manchester, R. N. 2006, MNRAS, 369, 655, doi: 10.1111/j.1365-2966.2006.10302.x

Johnston, S., & Romani, R. W. 2003, ApJL, 590, L95, doi: 10.1086/376826

Kim, M., & An, H. 2019, Journal of Korean Astronomical Society, 52, 41, doi: 10.5303/JKAS.2019.52.2.41

Kramer, M., Lyne, A. G., O'Brien, J. T., Jordan, C. A., & Lorimer, D. R. 2006, Science, 312, 549, doi: 10.1126/science.1124060

Kuiper, L., & Hermsen, W. 2009, A&A, 501, 1031, doi: 10.1051/0004-6361/200811580

Liu, Y., Keith, M. J., Antonopoulou, D., et al. 2024, MNRAS, 532, 859, doi: 10.1093/mnras/stae1499

Livingstone, M. A., Kaspi, V. M., Gavriil, F. P., et al. 2007, Ap&SS, 308, 317, doi: 10.1007/s10509-007-9320-3

Lorimer, D. R., & Kramer, M. 2004, Handbook of Pulsar Astronomy, Vol. 4

Luo, J., Ransom, S., Demorest, P., et al. 2021, ApJ, 911, 45, doi: 10.3847/1538-4357/abe62f

Lyne, A., Hobbs, G., Kramer, M., Stairs, I., & Stappers, B. 2010, Science, 329, 408, doi: 10.1126/science.1186683

Lyne, A. G., Jordan, C. A., Graham-Smith, F., et al. 2015, MNRAS, 446, 857, doi: 10.1093/mnras/stu2118

Manchester, R. N., Mar, D. P., Lyne, A. G., Kaspi, V. M., & Johnston, S. 1993, ApJL, 403, L29, doi: 10.1086/186714

Marshall, F. E., Guillemot, L., Harding, A. K., Martin, P., & Smith, D. A. 2015, ApJL, 807, L27, doi: 10.1088/2041-8205/807/2/L27

—. 2016, ApJL, 827, L39, doi: 10.3847/2041-8205/827/2/L39

Middleditch, J., & Pennypacker, C. 1985, Nature, 313, 659, doi: 10.1038/313659a0

Mignani, R. P., Shearer, A., de Luca, A., et al. 2019, ApJ, 871, 246, doi: 10.3847/1538-4357/aafb04

Parthasarathy, A., Johnston, S., Shannon, R. M., et al. 2020, MNRAS, 494, 2012, doi: 10.1093/mnras/staa882

Seward, F. D., Harnden, F. R., J., & Helfand, D. J. 1984, ApJL, 287, L19, doi: 10.1086/184388

Shaw, B., Stappers, B. W., & Weltevrede, P. 2018, MNRAS, 475, 5443, doi: 10.1093/mnras/sty160

Tuo, Y., Serim, M. M., Antonelli, M., et al. 2024, ApJL, 967, L13, doi: 10.3847/2041-8213/ad4488

Wang, L. J., Ge, M. Y., Wang, J. S., et al. 2020, MNRAS, 494, 1865, doi: 10.1093/mnras/staa884

Weisskopf, M. C., Soffitta, P., Baldini, L., et al. 2022, Journal of Astronomical Telescopes, Instruments, and Systems, 8, 026002, doi: 10.1117/1.JATIS.8.2.026002

Xie, F., Wong, J., La Monaca, F., et al. 2024, ApJ, 962, 92, doi: 10.3847/1538-4357/ad17ba

Young, N. J., Stappers, B. W., Lyne, A. G., et al. 2013, MNRAS, 429, 2569, doi: 10.1093/mnras/sts532

Zhang, W., Marshall, F. E., Gotthelf, E. V., Middleditch, J., & Wang, Q. D. 2001, ApJL, 554, L177, doi: 10.1086/321703